ChemPubSoc Europe

DOI: 10.1002/cctc.201900144

CHEMCATCHEM Communications

# Novel Supramolecular Photocatalyst Based on Conjugation of Cucurbit[7]uril to Non-Metallated Porphyrin for Electrophotocatalytic Hydrogen Generation from Water Splitting

Yogesh Kumar,[a, b] Bhushan Patil,[b] Aisan Khaligh,[a, b] Seyed E. Hadi,[b] Tamer Uyar,[b] and Dönüs Tuncel*[a, b]

Visible-light triggerable, stable, organic material-based photocatalysts that can function in alkaline media without the necessity of sacrificial agent for hydrogen production are highly sought after. Here, we report a novel supramolecular photocatalyst that confers the aforementioned features. This supramolecular photocatalyst (**TPP-4CB7**) is synthesized through the conjugation of monohydroxylated cucurbit(7)uril (CB7) hosts to a suitably substituted tetraphenyl porphyrin. Although **TPP-4CB7** by its own preforms as an efficient visible light triggered photocatalyst, the hydrogen production efficiency is significantly enhanced upon mixing with $TiO_2$. The resulting nanocomposite (**TPP-CB-$TiO_2$@Pt**) is observed to exhibit remarkable electrophotocatalytic activity under visible light and produces hydrogen (onset potential −10 mV, turn over frequency (TOF) 0.202 $s^{-1}$, 24.5 mmol $h^{-1}$ $g^{-1}$) from water splitting without any significant degradation during four runs (5 h each) in alkaline media and in the absence of sacrificial agent.

Photocatalytic water splitting has been demonstrated as a clean and simplest means for the conversion of solar energy into hydrogen fuel.[1] Although extensive research has been carried out to generate hydrogen from water splitting, sustainable production of hydrogen is still a great challenge. A number of photocatalytic systems have been developed during the past decade but those are mainly based on inorganic semiconductor materials.[2] Titanium oxide ($TiO_2$) is one of the widely used photocatalysts because of its high chemical stability, ambient operational conditions, strong oxidizing power of holes, non-toxicity and low cost.[3,4] However, there are some drawbacks in its use as a photocatalyst as it possesses a wide energy band gap (3.2–3.4 eV) and as a result of this it absorbs the light in the UV region and a fast recombination rate between photogenerated electron-hole pairs. To modify its band gap in order to enhance the light absorption ability in the visible region, it is often doped with various metals or dyes.[3–5] It is also possible to tune its photocatalytic activity by forming hybrid or nanocomposite materials with photosensitizers. However, in this case, the stability of the photosensitizer could be an issue. To this end, the quest for a newer and better photocatalyst that is both photoactive in the visible region of the spectrum and chemically stable is still under intense investigation.

Porphyrin and conjugated material-based organic frameworks and nanostructures recently started to appear in the literature as non-inorganic photocatalytic materials for water splitting to produce hydrogens and oxygens.[6–8] Porphyrin absorption spectra are characterized by strong Soret band absorbing in the region of 410–450 nm and Q bands centered between 500–700 nm. Due to its high molar absorptivity, dual-absorption band feature and high charge carrier mobility, the electron migrations are believed to be facilitated, thus reducing the risks of photogenerated electron-hole pairs recombination.[6b,c] In this regard, self-assembled porphyrin derivatives in the form of nanoparticles, nanowires and nanorods[9–11] as well as the composite of porphyrin-based porous covalent organic framework with $TiO_2$,[12] porphyrin-based imine gels[13] and cobalt porphyrin-polypyridyl surface coatings[14] were utilized as visible-light triggered photocatalysts in the hydrogen production from water splitting.

Herein, we report the synthesis of a novel photoactive supramolecular assembly that is based on the conjugation of cucurbit[7]uril hosts to free-base porphyrin core (**TTP-4CB7**) (Scheme 1) and also demonstrate the use of this assembly as a photocatalyst in hydrogen production from water splitting. Cucurbit[n]uril is a macrocycle and can be found in various sizes depending upon the number of glycol units which is composed of. It possesses a hydrophobic cavity and two hydrophilic portals that are decorated with carbonyl units. Due to these features, CBs can bind well with suitably sized hydrophobic molecules and form stable complexes. Among the CB family, cucurbit[7]uril (CB7), which contains seven glycol units, has good water solubility.[15] Host-guest chemistry of the CB homologues studied extensively, however, the studies involving

[a] Dr. Y. Kumar, Dr. A. Khaligh, Prof. D. Tuncel
Department of Chemistry
Bilkent University
Ankara 06800 (Turkey)
E-mail: dtuncel@fen.bilkent.edu.tr
[b] Dr. Y. Kumar, Dr. B. Patil, Dr. A. Khaligh, S. E. Hadi, Prof. T. Uyar, Prof. D. Tuncel
UNAM-National Nanotechnology Research Center, Institute of Materials Science and Nanotechnology
Bilkent University
Ankara 06800 (Turkey)

Supporting information for this article is available on the WWW under https://doi.org/10.1002/cctc.201900144


© 2019 Wiley-VCH Verlag GmbH & Co. KGaA, Weinheim

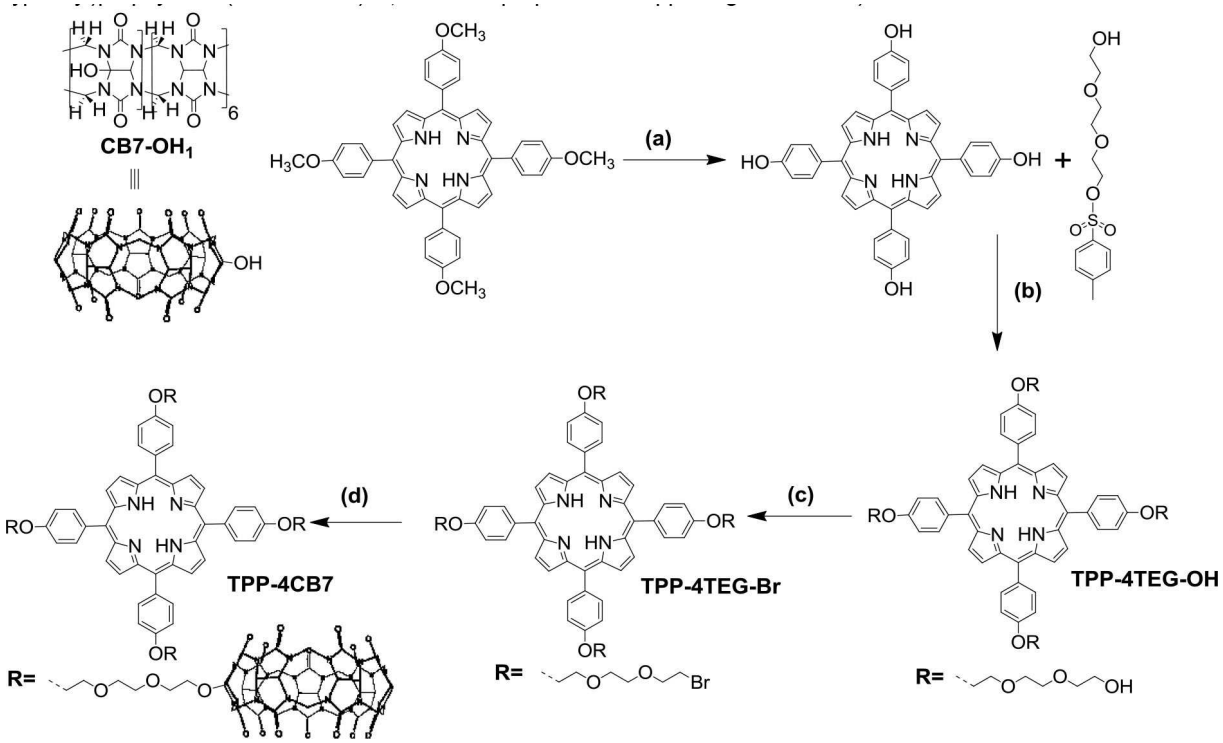


**Scheme 1.** Synthesis of **TPP-4CB7**: (a) $BBr_3$, $CH_2Cl_2$, 0 °C→1 h, 25 °C→48 h, 92%; (b) $K_2CO_3$, KI, DMF, 80 °C, 50 h, 90%; (c) $PPh_3$, $CBr_4$, $CHCl_3$, 0 °C→30 min, 25 °C→60 h, 68% ; (d) CB7-$OH_1$, DMSO, NaH, 0 °C→10 min, 25 °C→70 h, 72%.

the use of functionalized CB-homologues in the nanostructured materials are still limited.

In the literature, there are not many examples on the conjugation of functionalized CB to photoactive molecules and their applications. Moreover, to the best of our knowledge, this is the first example to CB-based photoactive supramolecular assembly that is employed in the photocatalytic hydrogen production.

Scheme 1 shows the structure of the assembly based on the conjugation of CB7 to porphyrin core (**TTP-4CB7**). Our design criteria take into accounts several important features: Non-metallated porphyrin core that will provide photoactivity for visible light absorption and charge separation; hydrophilic and flexible triethylene glycol linkers that can donate electrons and render the assembly water-miscible/hydrophilic; multi receptors (CB7) with carbonyl portals that will coordinate with water, metal co-catalysts (e.g. Pt and $TiO_2$) for efficient energy transfer and charge separation/stabilization as well as providing chemical stability to the assembly. Moreover, the cavities of CB7 are available to hold guests and produced $H_2$ gases.[16]

**TTP-4CB7** was synthesized according to the reaction scheme 1. Monohydroxy cucurbit[7]uril (**CB7-$OH_1$**) was synthesized from **CB7** following to the literature procedures.[17] The precursor porphyrin, 5,10,15,20-tetrakis(4-methoxyphenyl)porphyrin (**TPP-4$OCH_3$**),[18] was prepared according to literature precedents and then through demethylation of its methoxy groups using boron tribromide, tetraphenylporphyrin (**TPP-4OH**) was obtained. **TPP-4OH** was treated with excess monotosylated-TEG in the presence of potassium iodide and potassium carbonate at 80 °C to afford hydroxylated-TEG-porphyrin **TPP-4TEG-OH** which was subsequently converted into bromo-TEG-porphyrin **TPP-4TEG-Br** *via* Appel reaction in the presence of $CBr_4$ and triphenylphosphine. All of these porphyrin derivatives were fully characterized using $^1H$ and $^{13}C$ NMR and mass spectroscopy (see supporting information).

In the final step, **TPP-4CB7** was synthesized by the reaction of **TPP-4TEG-Br** with an excess of **CB7-$OH_1$** in the presence of NaH in DMSO. The progress of the reaction was monitored by mass spectroscopy to make sure all four arms of the porphyrin were functionalized with CB7. After the completion of the reaction, the product **TPP-4CB7** was isolated and purified by Sephadex G-25 column using water as eluent. After the removal of water, the greenish colored solid product was obtained which has a solubility in water with the concentration of around 0.2 mM.

**TPP-4CB7** was fully characterized by $^1H$-NMR, ESI-mass, UV-visible and IR spectrometry as shown in supporting information. In the ESI-MS spectrum, the related signals are readily assigned to corresponding molecular ions as doubly and triply charged ions as shown in supporting information. Although we have recorded its $^{13}C$-NMR spectrum, due to the limited solubility of the assembly and as $^{13}C$-NMR spectroscopy measurement requires a sample with high concentration, the spectrum is mainly dominated by the chemical shifts of CB7 and signals due to tetraphenyl porphyrin unit was not visible.

Figure 1 compares the $^1H$ NMR spectra of **TPP-4TEG-OH**, **TPP-4TEG-Br**, and **TPP-4CB7**. As can be seen in the $^1H$ NMR spectrum of **TPP-4CB7** in Figure 1A, although chemical shifts of


© 2019 Wiley-VCH Verlag GmbH & Co. KGaA, Weinheim

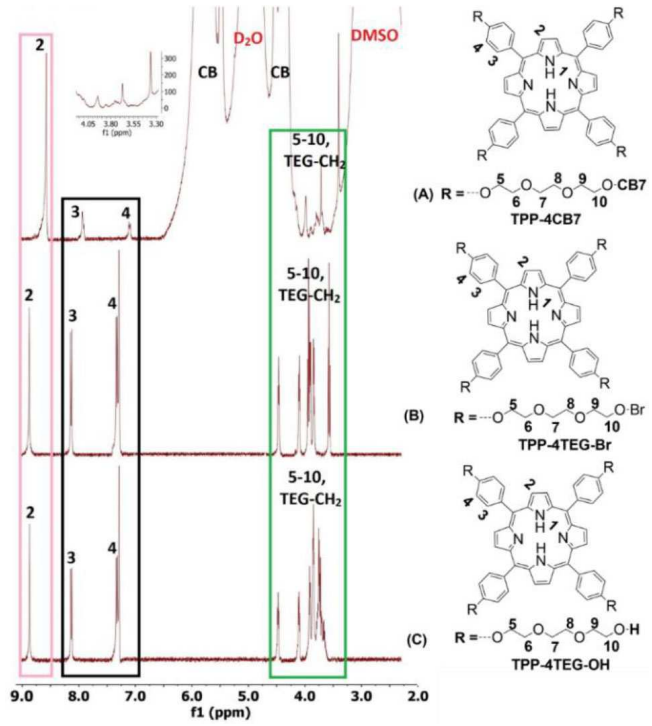


**Figure 1.** Comparison of $^{1}$H NMR (400 MHz, 25 °C) spectra of (A) **TPP-4CB7** (in $D_2O$, a few drops of DMSO-$d_6$), (B) **TPP-4TEG-Br** (in $CDCl_3$) and (C) **TPP-4TEG-OH** (in $CDCl_3$).

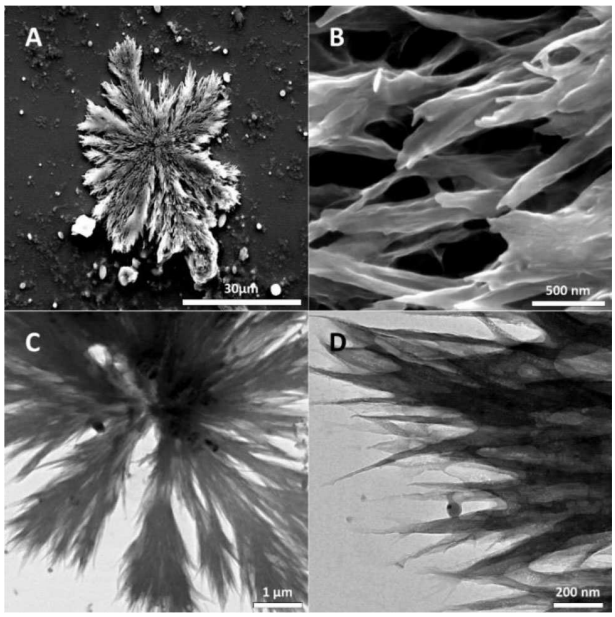


**Figure 2.** SEM (A and B) and TEM (C and D) images of **TPP-4CB7**.

CB7 protons are quite intense and dominating the spectrum because of its higher ratio in **TPP-4CB7**, still protons of tetraphenyl porphyrin and TEG linkers can be clearly identified further proving the formation of the desired compound.

Photophysical properties of **TPP-4CB7** in water were also investigated. Figure S20c shows an overlay of UV-Vis absorbance spectra of **TPP-4TEG-OH, TPP-4TEG-Br**, and **TPP-4CB7**. Soret band of **TPP-4CB7** ($\lambda_{max}$ at 435 nm) is broader and 11 nm red-shifted and its Q-bands ($\lambda_{abs}$ at 525, 565, 600 and 655 nm) are slightly more intense (especially the band at 655 nm) than those two porphyrins indicating the aggregate formation.

In order to reveal the morphology of the aggregates, we recorded their electron microscopy (SEM and TEM) micrographs. Their SEM (Figure 2A and B) and TEM (Figure 2C and D) images show feathers like ribbons and porous structures.

Nitrogen physisorption was performed at 77 K to shed light on the porous properties of **TPP-4CB7. TPP-4CB7** showed a Type IV isotherm according to the IUPAC classification. The surface area was then calculated with the help of the Brunauer–Emmett–Teller (BET) model was found to be 12.2 $m^2 g^{-1}$ and the total specific pore volume is 0.115 $cm^3 g^{-1}$ for **TPP-4CB7** possessing a narrow pore size distribution in the range of 2–6 nm with a peak maximum at 3.1 nm (Figure S22-S25). It was also revealed that **TPP-4CB7** is composed of agglomerated slit like particles, which was also confirmed by the TEM imaging.

Electrophotocatalytic hydrogen production ability of **TPP-4CB7**, its nanocomposite with $TiO_2$, as well as the precursor **TPP-4TEG-OH** have been investigated in the presence and absence of the sacrificial agent. The nanocomposite of **TPP-4CB7** with $TiO_2$ was prepared by grinding $TiO_2$ with **TPP-4CB7** with the ratio of 2:1.[20,21] By mixing **TPP-CB-$TiO_2$,** chloroplatinic acid (appx. 1%), water, ethanol, Nafion and ascorbic acid (used for some studies) and after sonicating this mixture, a homogeneous ink was obtained. Ink with known volume was coated on the FTO by drop casting method. The detailed procedure of the ink and FTO preparation were explained in the supporting information. After drying in the vacuum oven, the resulting electrode was fully characterized before the photocatalytic studies by using PXRD, XPS, and SEM (Figure S28–S29).

The electrochemical properties of nanocomposite **TPP-CB–$TiO_2$@Pt** were measured in a conventional three-electrode cell. The schematic design of the electrochemical cell in which **TPP-CB–$TiO_2$@Pt** coated FTO used as working electrode and commercial Pt mesh as counter electrodes is described in Figure 3. The system was exiled under vacuum for 30 min to

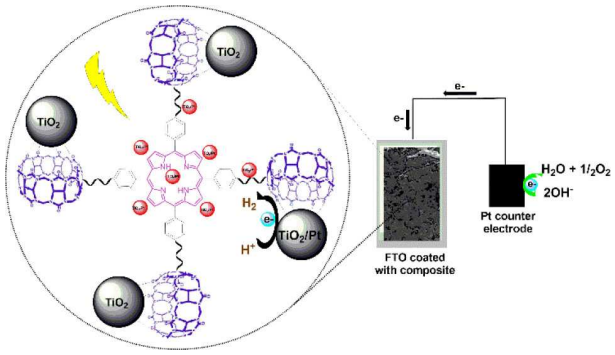


**Figure 3.** Schematic design of the electrochemical cell with **TPP-CB** coated FTO and commercial Pt mesh as working and counter electrodes.


© 2019 Wiley-VCH Verlag GmbH & Co. KGaA, Weinheim

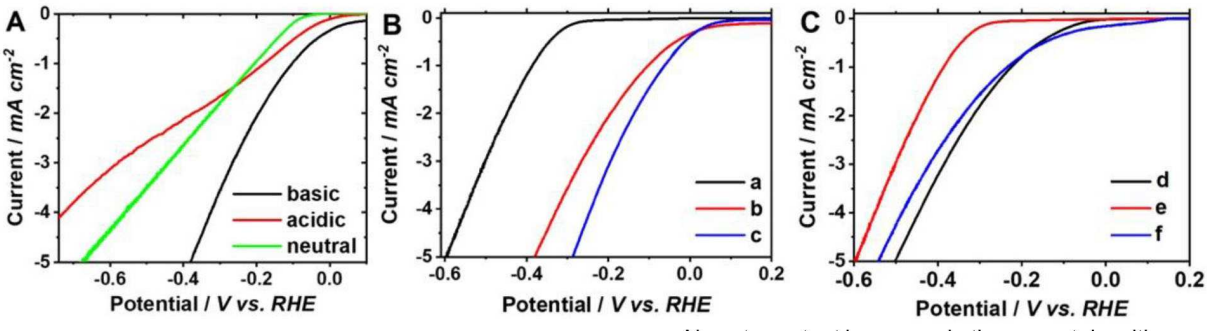


**Figure 4.** (**A**) Polarization curves of FTO electrodes coated with **TPP-CB-$TiO_2$@Pt** obtained under different media (acidic, 0.5 M $H_2SO_4$; neutral, 0.1 M PBS; basic, 0.1 M KOH); (**B** and **C**) Polarization curves of FTO electrodes coated with different films obtained under Ar saturated 0.1 M KOH with the scan rate 10 mV/s. a) $TiO_2$@Pt; b) TPP-CB-$TiO_2$@Pt; c) TPP-CB-$TiO_2$@Pt[a] without sacrificial agent; d) TPP-CB@Pt; e) TiO2@Pt; f) TPP-CB@Pt[a] without sacrificial agent. ([a] test 1: without the sacrificial agent)

eradicate the dissolved oxygen prior to the irradiation by a 300 W xenon arc lamp as a visible light source. The catalytic formation of hydrogen activated, resulting from the reduction of $H^+$ in $H_2O$ by electrons when a negative potential was applied to the working electrode. The electrons were moved from the Pt counter electrode to the composite coated FTO working electrode. The water molecule was oxidized on the Pt electrode to produce $O_2$.

In the photocatalytic system, a photocatalyst harvests sunlight and primarily acts as a photosensitizer for exciton generation. Conventionally, 10% efficient solar water-splitting devices should operate at 10 mA cm$^{-2}$ below ~0.45 V overpotential (η) for overall water splitting (i.e. oxygen evaluation reaction (OER) and hydrogen evaluation reaction (HER) combined).[3–5]

The photocatalytic ability of composite **TPP-CB-$TiO_2$@Pt** was first tested in three different media, acidic (0.5 M $H_2SO_4$), neutral (0.1 M PBS, pH 7.0) and basic (0.1 M KOH) (Figure 4A) and polarization curves, the onset potentials (at which the reduction is started) for the HER are measured. In acidic media, composite **TPP-CB-$TiO_2$@Pt** shows a low onset potential, (−44 mV), turnover frequency (TOF) (0.065 s$^{-1}$) (see supporting information Table S1) and poor stability because the catalyst was degraded in the first run of measurement.

In neutral media, the onset potential for the composite **TPP-CB-$TiO_2$@Pt** is observed at −30 mV with TOF 0.049 s$^{-1}$. Although the catalyst survives repeated cycles of measurements in the neutral medium, its TOF is rather low. On the other hand, the HER onset potential in a basic medium is observed at −30 mV with $\eta$@10, −0.607 V and higher TOF of 0.139 s$^{-1}$. These studies suggest that composite **TPP-CB-$TiO_2$@Pt** harvests sunlight and primarily acts as a good photosensitizer in basic media and it shows a higher photocatalytic performance and stability as compared to those of the acidic and neutral. The superior efficiency of the photocatalytic system in an alkaline medium can be explained as follows. In acidic medium, pyrrolic nitrogen of the porphyrin can be protonated and this, in turn, can decrease the interaction of Pt as well as the efficiency of charge separation. Moreover, in acidic medium TPP-CB assembly becomes more soluble and carbonyl groups of the CB coordinate with protonium ions by preventing the interaction of CB with $TiO_2$. On the other hand, in the alkaline medium porphyrin will be in its free base form and carbonyl groups of CBs available for co-ordination with $SiO_2$ and Pt.

Having the optimal conditions at hand, first, we examined the photocatalytic properties of **TPP-CB@Pt** and **$TiO_2$@Pt** systems in basic media in a similar way. **TPP-CB@Pt** and **$TiO_2$@Pt** produced a small amount of hydrogen having onset potential of −70 mV and −280 mV, respectively (Figure 4C). The overpotential ($\eta$@10) and TOF for **TPP-CB@Pt** is found at −0.75 V and 0.118 s$^{-1}$, respectively and for **$TiO_2$@Pt** at −0.81 V and 0.103 s$^{-1}$ respectively (Table S1).

However, the photocatalytic performance was found to be significantly enhanced in the case of composite **TPP-CB-$TiO_2$@Pt** as compared to photocatalytic activities shown by **$TiO_2$@Pt** and **TPP-CB@Pt. TPP-CB-$TiO_2$@Pt** produces hydrogen with an onset potential of −30 mV, TOF of 0.139 s$^{-1}$ and the overpotential ($\eta$@10) of 0.61 V. This is due to the synergistic influence of the combination of TPP-CB and $TiO_2$ into one system.[11,12] The polarization curves of FTO film electrodes under stable conditions are presented in Figure 4. The potential required to reach these expected current densities (i.e. $\eta$ @ 10 mA cm$^{-2}$/V for HER) based on the geometric area ($j_g$) were compiled in a table shown in the supporting information (Table S1 and Figure S30-S31).

The photocatalytic activity of composite **TPP-CB-$TiO_2$** was also examined in the absence of co-catalyst Pt and it produced a negligible amount of hydrogen with an onset potential of −670 mV. This indicates that the Pt as a co-catalyst improved the hydrogen generation of composite **TPP-CB-$TiO_2$**.

To understand the effect of CB7 s on the photocatalytic activity of **TPP-CB-$TiO_2$**, electrochemical properties of **TPP-TEG-OH-$TiO_2$@Pt** which does not contain CB7 s were studied. For this composite without CB7 s, the HER onset potential of −33 mV with the lower value of TOF (0.108 s$^{-1}$) was measured which clearly reveals that the presence of CB7 s improved the photocatalytic performance of composite **TPP-CB-$TiO_2$@Pt**. Moreover, the stability of composite **TPP-TEG-OH-$TiO_2$@Pt** without CB7 s is quite low as it is degraded over a very short period of time (appx. within 2 min) as compared to **TPP-CB-$TiO_2$@Pt**.


© 2019 Wiley-VCH Verlag GmbH & Co. KGaA, Weinheim

We have also studied the photocatalytic activities of **TPP-CB@Pt, TPP-TEG-OH-$TiO_2$@Pt**, **TPP-CB-$TiO_2$@Pt** in the absence of a sacrificial electron donor (ascorbic acid, AA). These samples were designated as test 1 and the results were tabulated in the Table S1 (supporting information). Most remarkably, it was observed that the composite **TPP-CB-$TiO_2$@Pt (test 1)** without sacrificial agent shows onset potential value for the HER at −10 mV, TOF of 0.202 $s^{-1}$ and the overpotential ($\eta$@10) of 0.47 V. Furthermore, its photocatalytic performance was found to be consistent and stable even after four consecutive cycles (5 h each). These results indicate that **TPP-CB-$TiO_2$@Pt (test 1)** show significantly higher catalytic activity than the other aforementioned systems. The reason of higher activity in the absence of sacrificial agent needs to be investigated further but we can speculate that in the absence of AA, carbonyl groups of CB7 s are probably coordinating with water molecules and directing them to the catalytic centers more efficiently for facile water-splitting than in the presence of AA.

The stability of **TPP-CB-$TiO_2$@Pt** was determined by chronoamperometry at the 0.3 V under dark and light periodically (Figure 5). The apparent increase in the current densities after

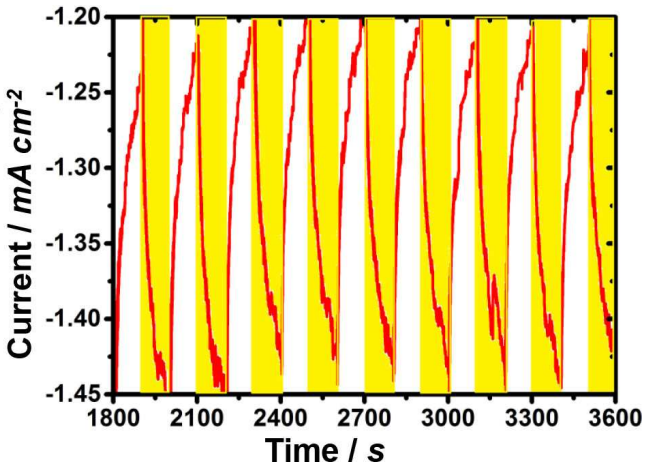


**Figure 5.** Chronoamperometry at 0.3 V vs. RHE in 0.1 M KOH under dark (represented by white color) and light (represented by yellow color) conditions.

light irradiation shows the efficiency of **TPP-CB-$TiO_2$@Pt** in the presence of photons.

Almost constant increases in the current densities were observed even after 1 h 30 min HER. The same electrode was further used for the durability of up to 6 h. To evaluate photocatalysis after 6 h stability polarization LSV were recorded (Figure S32) which clearly shows there is no significant change in the production of hydrogen.

Although, the onset potential and $\eta$@10 mA $cm^{-2}$ measured after 6 h (Figure S33) was slightly cathodic to 1$^{st}$ polarization curves of **TPP-CB-$TiO_2$@Pt** without the presence of ascorbic acid.

The morphology and elemental composition were analyzed before and after the 6 h experiment by SEM and XPS, respectively. The SEM showed that there was no significant change to the morphology of **TPP-CB-$TiO_2$@Pt** (Figure S35-S37). Peak fitting of various elements was also recorded after a 6 h-experiment using XPS spectrum with high-resolution scan (see supporting information, Figure S38). These analogous images indicate similar morphology before and after catalysis. In addition, XPS also shows the presence of Pt which proves that Pt is stable on the **TPP-CB-$TiO_2$**. The phase shift in XPS data of O(1 s) and Ti(2p) is possibly due to electrochemical, photocatalytic or interaction between **TPP-CB-$TiO_2$**, Pt and $TiO_2$.

The estimated amount of evolved hydrogen was also calculated by using Faraday law and $H_2$ producing equation. Details and a plot on which the results are summarized were given in the supporting information (Figure S39). The amounts of evolved hydrogen for **TPP-CB@Pt** in the presence and absence of AA were calculated to be 3.01 mmol $h^{-1}$ $g^{-1}$, 4.12 mmol $h^{-1}$ $g^{-1}$, respectively. For **TPP-CB-$TiO_2$@Pt** and **TPP-CB-$TiO_2$@Pt (test 1)**, amounts of hydrogens were calculated as 3.25 mmol $h^{-1}$ $g^{-1}$ and 24.5 mmol $h^{-1}$ $g^{-1}$. Faradaic efficiency (FE) was determined to be around 90%. Details of the FE determination was provided in the supporting information.

In conclusion, we have successfully synthesized a novel photoactive supramolecular assembly in which a tetraphenylporphyrin core is decorated with four of the receptor molecule, CB7. This assembly (**TPP-4CB7**) has an appreciable amount of water solubility and thus, can be used in many applications due to its distinctive features including combined photo and chemotherapy, chemo-/bio-sensors and photocatalysis. In this study, we have shown its ability as a photocatalyst in the hydrogen production from water splitting. Although **TPP-4CB7** by its own acts as a visible light triggered photocatalyst, its photocatalytic activity has enhanced significantly upon forming nanocomposite with $TiO_2$ as carbonyl portals of CB7 s act as anchoring groups and co-ordinate with $TiO_2$ to give rise homogenous mixture. The resulting nanocomposite, **TPP-CB-$TiO_2$@Pt**, is very efficient and stable photocatalyst and produces high amount of hydrogen (24.5 mmol $h^{-1}$ $g^{-1}$, onset potential −10 mV, TOF of 0.202 $s^{-1}$) without the necessity of extra sacrificial agent in alkaline media when compared to the similar photocatalysts reported in the literature as porphyrin organic polymer (5.602 mmol $h^{-1}$ $g^{-1}$)[12], porphyrin-based imine gel (0.095 mmol $h^{-1}$ $g^{-1}$)[13], g-$C_3N_4$/m-oxo dimeric Fe(III) porphyrin (0.0592 mmol),[22] Zn-porphyrin nanosheets (0.16 mmol $g^{-1}$ $h^{-1}$)[23] and benzobis(benzothiophene sulfone)-COF (16.3 mmol $h^{-1}$ $g^{-1}$).[8d]

## Experimental Section

The details on the synthesis of the precursor porphyrins and TPP-4CB7, electrophotochemical measurements, the related data, spectra are given in the supporting information part.


© 2019 Wiley-VCH Verlag GmbH & Co. KGaA, Weinheim

## Acknowledgements

*We thank The Scientific and Technological Research Council of Turkey-TÜBİTAK for funding (KBAG 215Z035).*

## Conflict of Interest

The authors declare no conflict of interest.

**Keywords:** cucurbituril · electrophotocatalytic hydrogen production · non-metallated porphyrin · supramolecular photocatalyst · water-splitting

[1] a) D. G. Nocera, *Acc. Chem. Res.* **2012**, *45*, 767; b) J. A. Turner, *Science* **2004**, *305*, 972; c) J. Barber, *Chem. Soc. Rev.* **2009**, *38*, 185.
[2] a) Y. Jiao, Y. Zheng, M. Jaroniec, S. Z. Qiao, *Chem. Soc. Rev.* **2015**, *44*, 2060; b) Y. Yan, B. Y. Xia, B. Zhao, X. Wang, *J. Mater. Chem. A* **2016**, *4*, 17587; c) M. G. Walter, E. L. Warren, J. R. McKone, S. W. Boettcher, Q. Mi, E. A. Santori, N. S. Lewis, *Chem. Rev.* **2010**, *110*, 6446; d) A. Paracchino, V. Laporte, K. Sivula, M. Gratzel, E. Thimsen, *Nat. Mater.* **2011**, *10*, 456; e) H. Tong, S. Ouyang, Y. Bi, N. Umezawa, M. Oshikiri, J. Ye, *Adv. Mater.* **2012**, *24*, 229.
[3] Y. Xu, C. Zhang, L. Zhang, X. Zhang, H. Yao, J. Shi, *Energy Environ. Sci.* **2016**, *9*, 2410.
[4] R. Asahi, T. Morikawa, H. Irie, T. Ohwaki, *Chem. Rev.* **2014**, *114*, 9824.
[5] Y. Xiang, X. Wang, X. Zhang, H. Hou, K. Dai, Q. Huang, H. Chen, *J. Mater. Chem. A* **2018**, *6*, 153.
[6] a) D. Gust, T. A. Moore, A. L. Moore, *Acc. Chem. Res.* **2009**, *42*, 1890; b) K. Ladomenou, M. Natali, E. Iengo, G. Charalampidis, F. Scandola, A. G. Coutsolelos, *Coord. Chem. Rev.* **2015**, *304–305*, 38; c) M. Urbani, M. Grätzel, M. K. Nazeeruddin, T. Torres, *Chem. Rev.* **2014**, *114*, 12330; d) L. Wang, R. Fernandez-Teran, L. Zhang, D. L. A. Fernandes, L. Tian, H. Chen, H. Tian, *Angew. Chem.* **2016**, *128*, 12494; e) P. B. Pati, G. Damas, L. Tian, D. L. A. Fernandes, L. Zhang, I. B. Pehlivan, T. Edvinsson, C. M. Araujo, H. Tian, *Energy Environ. Sci.* **2017**, *10*, 1372.
[7] a) S. Ghosh, N. A. Kouame, L. Ramos, S. Remita, A. Dazzi, A. Deniset-Besseau, P. Beaunier, F. Goubard, P. Aubert, H. Remita, *Nat. Mater.* **2015**, *14*, 505; b) H.-Q. Xu, J. Hu, D. Wang, Z. Li, Q. Zhang, Y. Luo, S. Yu, H.-L. Jiang, *J. Am. Chem. Soc.* **2015**, *137*, 13440; c) X. Wang, K. Maeda, A. Thomas, K. Takanabe, G. Xin, J. M. Carlsson, K. Domen, M. Antonietti, *Nat. Mater.*, **2009**, *8*, 76; d) L. Li, Z. Cai, Q. Wu, W. Lo, N. Zhang, L. X. Chen, L. Yu, Rational, *J. Am. Chem. Soc.* **2016**, *138*, 7681.
[8] a) R. S. Sprick, J. Jiang, B. Bonillo, S. Ren, T. Ratvijitvech, P. Guiglion, M. A. Zwijnenburg, D. J. Adams, A. I. Cooper, *J. Am. Chem. Soc.* **2015**, *137*, 3265; b) V. S. Vyas, V. W. Lau and B. V. Lotsch, *Chem. Mater.* **2016**, *28*, 5191; c) R. S. Sprick, B. Bonillo, R. Clowes, P. Guiglion, N. J. Brownbill, B. J. Slater, F. Blanc, M. A. Zwijnenburg, D. J. Adams, A. I. Cooper, *Angew. Chem.* **2016**, *128*, 1824; d) X. Wang, L. Chen, S. Y. Chong, M. A. Little, Y. Wu, W. H. Zhu, R. Clowes, Y. Yan, M. A. Zwijnenburg, R. S. Sprick, A. I. Cooper *Nat. Chem.* **2018**, *10*, 1180; e) K. Schwinghammer, S. Hug, M. B. Mesch, J. Senker, B. V. Lotsch, *Energy Environ. Sci.* **2015**, *8*, 3345.
[9] N. Zhang, L. Wang, H. Wang, R. Cao, J. Wang, F. Bai, H. Fan, *Nano Lett.* **2018**, *18*, 560.
[10] J. Wang, Y. Zhong, L. Wang, N. Zhang, R. Cao, K. Bian, L. Alarid, R. E. Haddad, F. Bai, H. Fan, *Nano Lett.* **2016**, *16*, 6523.
[11] D. Wang, L. Niu, Z.-Y. Qiao, D.-B. Cheng, J. Wang, Yong Zhong, F. Bai, H. Wang, H. Fan, *ACS Nano* **2018**, *12*, 3796.
[12] G. Mukherjee, J. Thote, H. B. Aiyappa, S. Kandambeth, S. Banerjee, K. Vanka, R. Banerjee, *Chem. Commun.* **2017**, *53*, 4461.
[13] P. Liao, Y. Hu, Z. Liang, J. Zhang, H. Yang, L.-Qi He, Ye.-X. Tong, J.-M. Liu, L. Chen, C.-Y. Su, *J. Mater. Chem. A*, **2018**, *6*, 3195.
[14] A. M. Beiler, D. Khusnutdinova, B. L. Wadsworth, G. F. Moore, *Inorg. Chem.* **2017**, *56*, 12178.
[15] a) D. Shetty, J. K. Khedkar, K. M. Park, K. Kim, *Chem. Soc. Rev.* **2015**, *44*, 8747; b) K. I. Assaf, W. M. Nau, *Chem. Soc. Rev.* **2015**, *44*, 394; c) S. J. Barrow, S. Kasera, M. J. Rowland, J. del Barrio, O. A. Scherman, *Chem. Rev.* **2015**, *115*, 12320; d) S. Gürbüz, M. Idris, D. Tuncel, *Org. Biomol. Chem.* **2015**, *13*, 330; e) A. Koc, D. Tuncel, *Isr. J. Chem.* **2018**, 58, 334.
[16] S. Pan, S. Mondal, P. K. Chattaraj, *New J. Chem.* 2013, **37**, 2492.
[17] a) A. Koc, R. Khan, D. Tuncel, *Chem. Eur. J.* **2018**, *24*, 15550; b) N. Dong, J. He, T. Li, A. Peralta, M. R. Avei, Mi. Ma, A. E. Kaifer, *J. Org. Chem.* **2018**, *83*, 5467; c) Y. Ahn, Y. Jang, N. Selvapalam, G. Yun, K. Kim, *Angew. Chem. Int. Ed.* **2013**, *52*, 3140.
[18] a) D. Tuncel, N. Cındır, U. Koldemir, *J. Inclusion Phenom. Macrocyclic Chem.* **2006**, *55*, 373; b) L. Wen, M. Li and J. B. Schlenoff, *J. Am. Chem. Soc.* **1997**, *119*, 7726.
[19] D. P. Dubal, G. S. Gund, R. Holze, H. S. Jadhav, C. D. Lokhande, C. J. Park, *Dalton Trans.* **2013**, *42*, 6459.
[20] C. Xu, S. De, A. M. Balu, M. Ojedad, R. Luque, *Chem. Commun.* **2015**, *51*, 6698.
[21] M. F. Tovini, B. Patil, C. Koz, T. Uyar, E. Yılmaz, *Nanotechnology* **2018**, *29*, 475401.
[22] D. H. Wang, J. N. Pan, H. H. Li, J. J. Liu, Y. B. Wang, L. T. Kang, J. N. Yao, *J. Mater. Chem. A* **2016**, *4*, 290.
[23] H. Li, L. Jie, J. Pan, L. Kang, J. Yao, *J. Mater. Chem. A* **2016**, *4*, 6577.

Manuscript received: January 24, 2019
Revised manuscript received: April 17, 2019
Accepted manuscript online: April 22, 2019
Version of record online: May 20, 2019


© 2019 Wiley-VCH Verlag GmbH & Co. KGaA, Weinheim